BAB

287

Met O 11 Technical Note No. 163

Further solutions to the two-dimensional deformation model

M J P Cullen

Meteorological Office (Met O 11)
London Road
Bracknell
Berkshire
U.K.

January 1983

FH2A

Summary

A previous paper by the author discussed solutions to the deformation model of Hoskins and Bretherton between rigid boundaries with zero potential vorticity. In this paper the explicit construction method used there is extended to the free surface case, the difference between the solutions obtained, and finite difference solutions of the primitive equations, is similar to that with rigid boundaries. A finite difference method for the semigeostrophic equations is described and shown to converge to the solution given by the explicit construction. This method is then used to compare solutions of the semi-geostrophic and primitive equations using data with non-zero potential vorticity, including a representation of the stratosphere.

1. Introduction

A previous paper by the author, Cullen (1982), referred to henceforward as C, discussed solutions to the deformation model of frontogenesis introduced by Hoskins and Bretherton (1972), referred to as HB. It was shown that solutions could be obtained beyond the formation of a discontinuity by assuming the validity of the Lagrangian conservation laws for potential temperature and absolute momentum, incompressibility of the flow, and the geostrophic jump conditions introduced originally by Margules. Solutions obtained by adding artificial viscosity to the primitive equations and refining the mesh to convergence appeared to differ from the Lagrangian solution in the vertical structure of the front. The scale analysis described in HB and set in a more general context in a review paper by Hoskins (1982) suggests that the semigeostrophic approximation remains valid for longer than the no mixing approximation made by omitting dissipation from the equations. This means that the solution obtained as the inviscid limit of the semigeostrophic equations may be more physically relevant than the inviscid limit of the primitive equations. Whether this is true can only be determined by experiment. Mathematically it can only be shown that the two limits

are different.

In this paper the work described in C is extended in several ways, in order to solve more of the cases described in HB after discontinuities have formed. The first extension is to include the correct lower boundary conditions which allows the effect of surface pressure variations to be included. The scale analysis of HB suggests that this only has a small effect. However, since including it adds another small parameter to the system, there is a danger that singular effects may occur. The explicit construction used in C is extended by iteration to include this case and the differences between it and a finite difference solution to the primitive equations are shown to be no greater than before.

The logic in the explicit construction method is very complicated and it proved impracticable to use it to study problems with non-zero potential vorticity. Recently, however, the construction has been generalised by Purser and Cullen (1983). It is possible to show by qualitative arguments what the likely effects are. The more general construction has not yet been implemented, however. The finite difference primitive equations model was therefore modified to solve the semigeostrophic equations instead. This is difficult because the ageostrophic circulation is described by a parabolic equation once the discontinuity has formed. The problem with zero potential vorticity is solved by this method to check that it agrees with the explicit construction. The correct solution is obtained but the rate of convergence is very slow.

The two finite difference models are then used to compare solutions obtained with non-zero potential vorticity, including one with a discontinuity in potential vorticity to represent the tropopause. In HB it was found that folding of the tropopause prevents formation of a discontinuity there. This is confirmed. Differences between the semi-geostrophic and primitive equation solutions are similar to those observed in the test case in C. The errors close to the frontal surface appear to be dominated by the resolution. There are also differences in

the slopes of the isotherms above and below the frontal surface. These are insensitive to further increases in resolution and thus indicate that the solutions are genuinely different. It is possible to obtain sharper fronts from the semi-geostrophic model because the artificial viscosity can be reduced to lower values than in the primitive equation model. This is because of the separation of the calculation of geostrophic and ageostrophic winds. Care has thus to be taken not to allow the Richardson numbers to become unrealistically low.

2. Implementation of correct lower boundary conditions

Following HB and C we use the following set of two-dimensional equations:

$$\frac{\partial \phi}{\partial x} - fv = 0$$

$$\frac{Dv}{Dt} + \alpha v + f(u + \alpha x) = 0$$

$$\frac{D\theta}{Dt} = 0 \qquad (1)$$

$$\frac{\partial u}{\partial x} + \alpha + \frac{\partial w}{\partial z} = 0$$

$$\frac{\partial \phi}{\partial z} = g\theta/\theta_0$$

where the vertical coordinate z is defined by

$$z = \left[1 - \left(p/p_0\right)^{\frac{\gamma-1}{\gamma}}\right] \frac{\gamma}{\gamma-1} H_s \qquad (2)$$

The "rigid wall" boundary conditions are that $w = 0$ on $z = 0, H_a$ where $H_a = \gamma H_s/(\gamma-1)$ The f plane and Boussinesq approximations have been made. The equations are solved in $-L \leq x \leq L$. The lateral boundary conditions are as in C. The system (1) implies the following Lagrangian conservation laws.

$$\frac{DM}{Dt} + \alpha M = 0$$

$$\frac{D\theta}{Dt} = 0 \qquad (3)$$

$$\frac{DA}{Dt} + \alpha A = 0$$

where M is the absolute momentum (v+fx) and A is the area of a fluid element in the (x,z) plane. It was shown in C that a solution of (3) with zero potential vorticity could be constructed after a front has formed by assuming M and θ to be constant on fluid elements and using the jump condition

$$S = \frac{g}{f\theta_0} \frac{[\theta]}{[M]} \qquad (4)$$

for the slope S in the (x,z) plane of the line separating elements with values of θ differing by $[\theta]$ and values of M differing by $[M]$.

The boundary condition at $z = H_a$ corresponds to a condition at $p = 0$. That at $z=0$ corresponds to a condition at $p = p_0$. Variation in surface pressure, p_*, requires the lower boundary condition

$$\frac{\partial p_*}{\partial t} + u \frac{\partial p_*}{\partial x} = - \frac{p_* w}{H_s} \qquad (5)$$

and the geostrophic balance condition requires

$$fv = g \frac{\partial \phi_*}{\partial x} = RT \frac{\partial}{\partial x}(\ln p_*) \qquad (6)$$

where ϕ_* is the geopotential of the surface $z = 0$. We then approximate the condition (5) by

$$\frac{\partial \phi_*}{\partial t} + u \frac{\partial \phi_*}{\partial x} = -gw = -\alpha H_a - g\int_0^{H_a} \frac{\partial u}{\partial x} dz \qquad (7)$$

The implementation of condition (7) in the semi-implicit primitive equation scheme used in C is straightforward. The time derivatives in (7) and the full x momentum equations are represented by:

$$\delta_t \bar{u}^t + \left(u\frac{\partial u}{\partial x} + w\frac{\partial u}{\partial z} + \frac{\partial}{\partial x}(\phi - \phi_*) - fv \right)_t + \overline{\frac{\partial \phi_*}{\partial x}}^{2t} = 0 \qquad (8)$$

$$\delta_t \bar{\phi}_*^t + \left(u\frac{\partial \phi_*}{\partial x} + \alpha H_a \right)_t + g\int_0^{H_a} \overline{\frac{\partial u}{\partial x}}^{2t} dz = 0$$

These equations are reduced to a Helmholz equation for ϕ_* in the usual way. The boundary conditions in x are that

$$\frac{\partial \phi_*}{\partial x} = 0 \qquad \text{on} \quad x = \pm L \qquad (9)$$

and the solution is then obtained by standard methods.

Implementation of the condition (7) in the explicit construction used in C requires the prior knowledge that the solution will be close to the rigid wall solution. The scale analysis of HB supports this. The logic of the construction becomes too difficult if the solution is not symmetrical, as happens once (7) is used. Therefore we first obtain the rigid wall solution and modify it, assuming that there is no change in the topology of the segments of constant M and θ. This is done as follows:

i. Assume that ϕ_* is given by (6) at t = 0.

ii. Evaluate v(z = 0) from the rigid wall solution at $t = \Delta t$.

iii. Calculate the implied ϕ_* from (6) at $t = \Delta t$.

iv. Calculate the change in ϕ_* over the interval Δt.

v. Modify the areas of the segments to be consistent with mass flow across z = 0 given by step (iv), allowing for the horizontal advection of ϕ_*.

vi. Go back to step (ii) and repeat till convergence.

In practice one pass through this logic is sufficient where Δt is the interval between output times (3 hours in C). The initial condition (6) for ϕ_* is also used for the finite difference integration.

3. Solution of the semi-geostrophic equations

When solving the system (3) in all but the simplest cases the direct geometrical construction used in C appears impracticable. This is because of the essential nonlinearity, that the slopes of the boundaries between segments depend on which segments adjoin; and that cannot be determined in advance. It should, however, be possible to use the general construction of Purser and Cullen (1983). In HB and the subsequent work reviewed by Hoskins (1982) the solutions were obtained by a coordinate transformation which made the problem linear in geostrophic coordinates.

$$X = x + f^{-1}v$$
$$Y = y - f^{-1}u \qquad (10)$$

The solution becomes discontinuous in physical space in finite time, but at this time it is still continuous in (X,Y) space. Therefore the solution using the coordinate transformation will apparently continue to exist, until the reverse transform to physical space is attempted. It is clear that the reverse transform will yield multi-valued results, which can be regularised by imposing a frontal surface in physical space and making a correct choice of values on either side of it. However, this procedure will violate the conservation of mass of fluid elements since the areas of some elements will be reduced in the regularisation. Thus this procedure will not give the solution obtained by the explicit construction which took mass conservation into account. It is not clear how to modify it without losing the simplicity of the equations in (X,Y) coordinates.

We therefore use a more direct approach in this paper. The equations are split as follows:

$$\frac{\partial v_g}{\partial t} - \alpha x \frac{\partial v_g}{\partial x} + \alpha v_g = 0$$

$$\frac{\partial \theta}{\partial t} - \alpha x \frac{\partial \theta}{\partial x} = 0 \qquad (11)$$

which includes the geostrophic advection, and, iteratively,

$$\frac{\partial u_{ag}}{\partial \tau} = f v_g - \frac{\partial \phi}{\partial x} + K_1 \frac{\partial^2 u_{ag}}{\partial x^2}$$

$$\frac{\partial v_{ag}}{\partial \tau} + u_{ag} \frac{\partial v_g}{\partial x} + w_{ag} \frac{\partial v_g}{\partial z} + f u_{ag} = K_2 \frac{\partial^2 v}{\partial x^2} \qquad (12)$$

$$\frac{\partial \theta}{\partial \tau} + u_{ag} \frac{\partial \theta}{\partial x} + w_{ag} \frac{\partial \theta}{\partial z} = K_2 \frac{\partial^2 \theta}{\partial x^2}$$

where $\frac{\partial u_{ag}}{\partial x} + \frac{\partial w_{ag}}{\partial z} = 0 \quad ; \quad w_{ag} = 0 \quad \text{at} \quad z = 0, H$

The step (12) is repeated to convergence with τ being an iteration time scale. After each timestep of length Δt of the calculations (11), it is found that (12) must be integrated for a "time" much greater than Δt to obtain convergence. The adjustment is carried out by linear waves which are damped by the use of a large coefficient K_1 in the equation for u_{ag}. The artificial viscosity K_2 which captures the discontinuity in v_g and θ should be very small. The need for a long adjustment time suggests that information has to be transmitted much faster than the speeds of the internal gravity waves used to carry out the adjustment in (12).

The behaviour of this iteration and its difference from a direct solution of the primitive equations are best discussed by analysing the equation for the (x,z) ageostrophic circulation. Consider the semi-geostrophic equations (1). The continuity equation implies that u and w can be represented in terms of a streamfunction ψ by

$$u = -\alpha x - \frac{\partial \psi}{\partial z}$$

$$w = \frac{\partial \psi}{\partial x} \qquad (13)$$

Then the equations for $\frac{\partial v}{\partial t}$ and $\frac{\partial \theta}{\partial t}$, together with the condition for geostrophic balance and the hydrostatic equation, determine ψ implicitly by the equation

$$f\frac{\partial}{\partial z}\left[\left(-\alpha x - \frac{\partial \psi}{\partial z}\right)\frac{\partial M}{\partial x} + \frac{\partial \psi}{\partial x}\frac{\partial M}{\partial z} + \alpha M\right] = \frac{g}{\theta_0}\frac{\partial}{\partial x}\left[\left(-\alpha x - \frac{\partial \psi}{\partial z}\right)\frac{\partial \theta}{\partial x} + \frac{\partial \psi}{\partial x}\frac{\partial \theta}{\partial z}\right] \qquad (14)$$

It is well known that this equation changes type according to the sign of the potential vorticity

$$q = -\frac{\partial M}{\partial z}\frac{\partial \theta}{\partial x} + \frac{\partial M}{\partial x}\frac{\partial \theta}{\partial z} \qquad (15)$$

being elliptic, parabolic or hyperbolic according as to whether q is positive, zero or negative. The discriminant of equation (14) is, in fact,

$$\left(\frac{g}{\theta_0}\frac{\partial \theta}{\partial x} + f\frac{\partial M}{\partial z}\right)^2 - 4f\frac{\partial M}{\partial x}\cdot\frac{g}{\theta_0}\frac{\partial \theta}{\partial z} \qquad (16)$$

Consider the case where a discontinuity forms. Then $\frac{\partial M}{\partial x}$, $\frac{\partial M}{\partial z}$, $\frac{\partial \theta}{\partial x}$ and $\frac{\partial \theta}{\partial z}$ all tend to infinity, but in the fixed ratio

$$1 : S : \frac{f\theta_0 S}{g} : \frac{f\theta_0 S^2}{g}$$

where S is the slope of the front. Substituting these ratios into (16) gives zero. This suggests that the (x,z) circulation may exhibit parabolic behaviour in the presence of a discontinuity, though equation (14) is no longer meaningful in this limit. This question requires further, more rigorous, study.

The rate at which information can be transferred by the (x,z) circulation depends on the eigenvalues of (14). When (14) becomes parabolic, information can be transmitted instantaneously. Thus, in the case of zero potential vorticity, it is known that information can be transmitted immediately between the boundaries of the problem. Similarly at a front, it may be necessary to transmit information infinitely fast along the frontal surface.

By using the iteration scheme (11), (12) to solve the semi-geostrophic equations we are imitating the adjustment carried out by the primitive equations, but by repeating to convergence we allow information to be transmitted an arbitrary distance. In practice, this is difficult to achieve. The use of (11) and (12) means that information will be transferred at the gravity wave speeds of the model. Typical speeds (Temperton and Williamson (1981)) show only the external mode and the first five internal modes travelling at more than $10ms^{-1}$. In order to solve the deformation problem in C correctly it is necessary to transfer information across half the width of the frontal zone at each time step, in order to maintain the correct frontal structure. In the problem solved in C, this distance is about $2x10^5$ m at 14 hours which is the time at which the results were presented. Equations (11) and (12) must be iterated for an effective time of $2x10^4$ sec at each timestep in order to achieve the transfer at $10ms^{-1}$. Since the timestep limit for the iteration is determined by the first internal mode speed of $100ms^{-1}$, about 200 iterations will be required using the low

resolution grid of C with $\Delta x = 10^4$m. Clearly these figures are only rough estimates, since it is not clear how many modes are required to represent the solution described in C accurately. The integrations discussed in section 4 used 75 iterations, after which further iterations had little effect. One of the reasons for the failure of the primitive equation solution to converge thus appears to be the inability to transfer information fast enough when discontinuities have formed. In the atmosphere, information can be transferred faster by sound waves, and also it is possible that waves may be trapped in the frontal zone and transmit information very fast during it. In view of this argiment, the zero potential vorticity problem solved in C would appear to be the severest possible test, and it is of interest to see how far the differences between the solutions obtained in that case persist with non zero potential vorticity. Several such cases are examined in the next section.

This discussion also shows how difficult it is to devise a successful procedure for solving the semi-geostrophic system. A direct method would have to move some fluid elements a large distance, and the nonlinearity inherent in the dependence of the slope of an inter-element boundary on the values of M and θ in the element is likely to prevent this being achieved except in very simple cases like that solved in C. The iteration (11), (12) could be speeded up by successively eliminating internal gravity modes from $\frac{\partial u}{\partial t}$ and increasing the time step. (This is essentially a multigrid technique). Alternatively (11) and (12) could be replaced by nonhydrostatic equations, and integrated explicitly. It is not clear whether the faster transfer rate would compensate for the greatly reduced iteration timestep, and limited experiments did not show any improvement in the results.

The results discussed in section 4 use the lower boundary condition (6). In the iteration scheme (12) the boundary conditions on the continuity equations are replaced by

$$w_z = 0 \quad \text{at} \quad z = H$$
$$= g^{-1}\left(\frac{\partial \phi_*}{\partial t} + u\frac{\partial \phi_*}{\partial x}\right) \quad \text{at} \quad z = 0 \qquad (17)$$

where ϕ_* is the geopotential at z = 0, satisfying the condition

$$fv|_{z=0} = \frac{\partial \phi_*}{\partial x} \qquad (18)$$

This results in a scheme for predicting surface pressure similar to that proposed by Browning and Kreiss (1982) using multiple time-scale arguments.

4. Results

In this section we show results from three experiments. The first solves equations (1) using the same data as in C with

$$u = -\alpha x$$
$$v = f(X(x,z) - x)$$
$$\theta = \theta_0 + \theta_1 \tan^{-1}\left(\frac{SX(x,z)}{L}\right)$$

where
$$\frac{x - X(x,z)}{z - \tfrac{1}{2}H} = -\frac{S g \theta_1}{\theta_0 L f^2}\,\frac{1}{\left(1 + \left(\frac{SX(x,z)}{L}\right)^2\right)}$$

and boundary conditions

$$w = 0 \quad \text{at} \quad z = H$$
$$gw = \frac{\partial \phi_*}{\partial t} + u.\nabla\phi_* \quad \text{at} \quad z = 0$$
$$u = \mp \alpha L \quad \text{at} \quad x = \pm L$$
$$v + fx = (\pm fL)e^{-\alpha t}$$
$$\theta = \theta_0 \pm \theta_1 \tan^{-1}(S)$$

The first series of experiments compares the finite difference primitive equation (PE) model using the boundary condition (6) with the explicit construction method modified to use the same boundary condition as described in section 2; and with the finite difference semi-geostrophic (SG) model described in section 3. The results for potential temperature, the V component of velocity, and the vertical velocity w, are shown in Figs. 1 to 8. The differences between the PE solution and the explicit construction are similar to those in C with the rigid wall conditions. The potential temperature comparison (Figs. 1 and 3) show that the slopes of the lines disagree above and below the frontal surface as well as in the region of strong contrast near $z = \frac{1}{2}H$. The SG model (Fig 6) agrees with the explicit construction except near $z = \frac{1}{2}H$. Convergence is very slow there because the discrete grid cannot define the slope accurately. The differences between the predictions of v velocity (Figs. 2, 4 and 7) are less obvious. The contours of large v in Figs 2 and 7 (SG) are more sharply peaked than in Fig 4 (PE), and the minimum value of $|v|$ on the boundary on the outside of the frontal region is about $1ms^{-1}$ in the semi-geostrophic integrations and $2ms^{-1}$ in the primitive equation integration. The vertical velocities (Figs 5 and 8) are greater in the PE integration. In the SG model, most of the large values are concentrated near the intersection of the front with the boundaries.

In Fig 9 some further diagnostics are shown. The first is the slope of the $\theta' = 0$ isotherm. In the exact solution this is much greater in the middle tropopause than where it is embedded in the frontal surface. The two finite difference models (using the same resolution) fall short of the maximum slope by the same amount, but the SG model gives a greater variation in slope with height. The second graph shows the position of maximum temperature gradient. The PE model is closer to the explicit construction. This position is considerably influenced by the effect of the artificial viscosity, and so is not a very reliable guide to accuracy. The third graph shows the implied

surface pressure. In this case the SG model is closer to the exact construction.

These results indicate that the SG finite difference model is converging to the solution given by exact construction as the mesh is refined. Convergence is very slow near the frontal surface. Using a 100 x 10 grid the maximum slope is 41, with 100 x 20 it is 46. The slopes of the isotherms above the below the frontal surface are essentially correct on the 200 x 20 grid. The PE model gives similar results in the frontal zone itself, but inaccurate slopes above and below the frontal surface. The strongest gradients are concentrated closer to the boundary.

In Figs 10 to 13 we show the results using uniform non-zero potential vorticity. The same resolution is used for both finite difference models. The differences between the θ fields are similar to those with zero potential vorticity. The strongest gradients are concentrated near the boundary in the PE model and the variation of slope with height is greater in the SG model. The v fields (Figs. 11, 13) show that the long-front winds are less near the boundaries away from the front, but greater in the jet maximum close to the front. The latter difference may reflect only the reduced viscosity in the SG solution.

In Figs. 14 to 17 the initial data has zero potential vorticity except in the top quarter of the domain where it is large and positive. This is intended as a comparison with the results of HB on upper tropospheric fronts. In agreement with HB, no discontinuity is formed at the tropopause. There are differences in the slopes of the isotherms in the lower half of the fields. Both models produce statically unstable solutions just below the tropopause. This is likely to be caused by vertical truncation errors near the sharp discontinuity of temperature gradient. The problem is worse in the SG integration.

The velocity fields (Figs. 15 and 17) show a well developed jet just below the tropopause with another maximum at the upper boundary. The maximum values of the jet core and of velocity gradients are greater in the SG model, probably because of reduced diffusion. There are again disagreements between the solutions near the upper and lower boundaries away from the frontal regions. The area enclosed by the $2ms^{-1}$ isotach is greater in the PE model.

5. Discussion

The results in this note show that the exact Lagrangian solution of the inviscid semi-geostrophic equations introduced in C can be obtained as a limit of a standard finite difference approximation to the SG equations as the mesh is refined and the artificial viscosity reduced. The solutions obtained using the primitive equations with artificial viscosity are slightly different away from the frontal surface. The errors in the jets and in the frontal surface appear to be dominated by finite difference truncation errors.

It is interesting to note that the primitive equation model appears unable to propagate a discontinuity into the fluid interior. A theorem proved by HB from the Eulerian equations assuming smooth solutions states that discontinuities can only form at the boundary. Purser and Cullen (1983) show that, after a discontinuity has formed, and the equivalence of the Eulerian and Langrangian forms of the equations may have been lost, that discontinuities can propagate in from the boundary and the potential circulation round a contour crossing the front is no longer conserved. It thus appears that the PE model may be trying to conserve potential circulation round all contours, and thus not allow the discontinuity to propagate into the domain. This can only be done by violating one of the Lagrangian conservation laws and thus obtaining a different solution from the explicit construction.

Another way of looking at the differences between the models is in terms of the effective rate of transfer of information by internal waves. The SG model requires information to be transmitted faster than the phase speed of linear internal gravity waves.

This note thus strengthens the impression that the PE and SG solutions are different, and that experiments should be carried out to test their physical validity. It is possible that the differences in the solutions might be greater in three dimensional models, where there is much greater freedom.

References

G Browning and H O Kreiss SIAM J. Appl. Math. 42 (1982), 704-718.

M J P Cullen Met O 11 Tech. Note No. 160 (1982).

B J Hoskins Ann. Rev. Fluid Mech. 14 (1982), 131-151.

B J Hoskins and F P Bretherton J. Atmos. Sci. 29 (1972), 11-37.

R J Purser and M J P Cullen Met O 11 Tech. Note No. 162 (1983).

C Temperton and D L Williamson Mon. Weath. Rev. 109 (1981), 729-757.

Fig. 1 Potential temperature after 13.9hr, explicit construction with free surface.

Fig. 2 y-velocity after 13.9hr, explicit construction.

Fig. 3 Potential temperature after 13.9hr, finite difference primitive equation, 200 x 40 grid, $K = 1.25 \times 10^4\ m^2 s^{-1}$.

Fig. 4 y velocity after 13.9hr, model as Fig. 3.

Fig. 5 Vertical velocity after 13.9hr, model as Fig. 3.

Fig. 6 Potential temperature after 13.9hr, finite difference semi-geostrophic model, 200 x 20 grid, $K = 600\ m^2 s^{-1}$.

Fig. 7 y velocity after 13.9hr, model as Fig. 6.

Fig. 8 Vertical velocity after 13.9hr, model as Fig. 6.

Fig. 9 Further diagnostics from solution after 13.9hr. In each case:

A Explicit construction.

B Finite difference (primitive equation).

C. Finite difference (semi geostrophic).

a. Slope of $\Theta = \Theta_o$ isotherm.

b. Position of maximum $\frac{\partial \theta}{\partial x}$ for given z.

c. Surface pressure.

Fig. 10 Potential temperature after 13.9hr, model as Fig. 3 (except 200 x 20 grid), data set with uniform nonzero potential vorticity.

Fig. 11 y velocity after 13.9hr, model and data as Fig. 10.

Fig. 12 Potential temperature after 13.9hr, model as Fig. 6, data as Fig. 10.

Fig. 13 y velocity after 13.9hr, model as Fig. 6, data as Fig. 10.

Fig. 14 Potential temperature after 13.9hr, model as Fig. 10, data set with discontinuity in potential vorticity.

Fig. 15 y velocity after 13.9hr, model and data as Fig. 14.

Fig. 16 Potential temperature after 13.9hr, model as Fig. 6, data as Fig. 14.

Fig. 17 y velocity after 13.9hr, model as Fig. 6, data as Fig. 14.

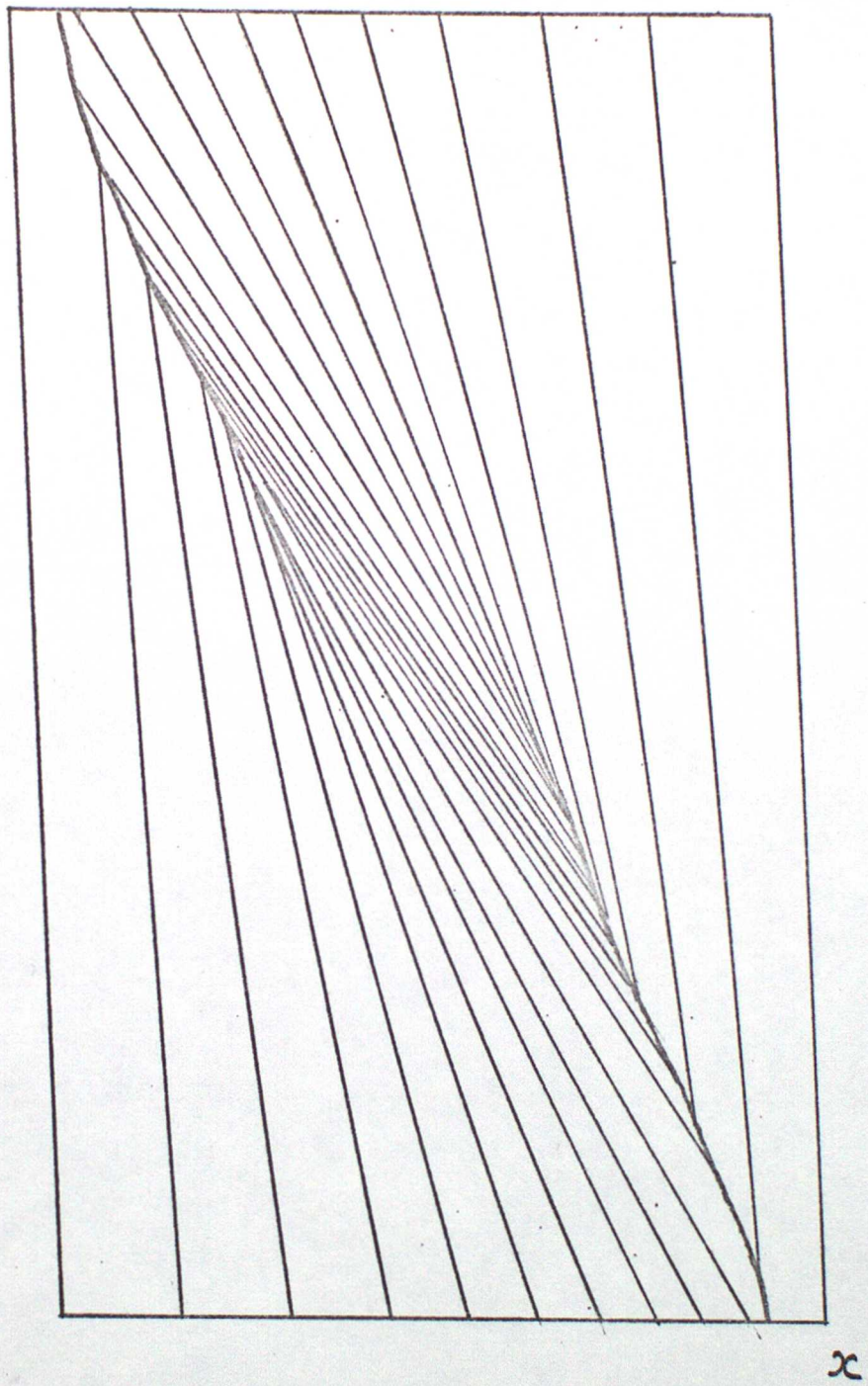

FIG. 1

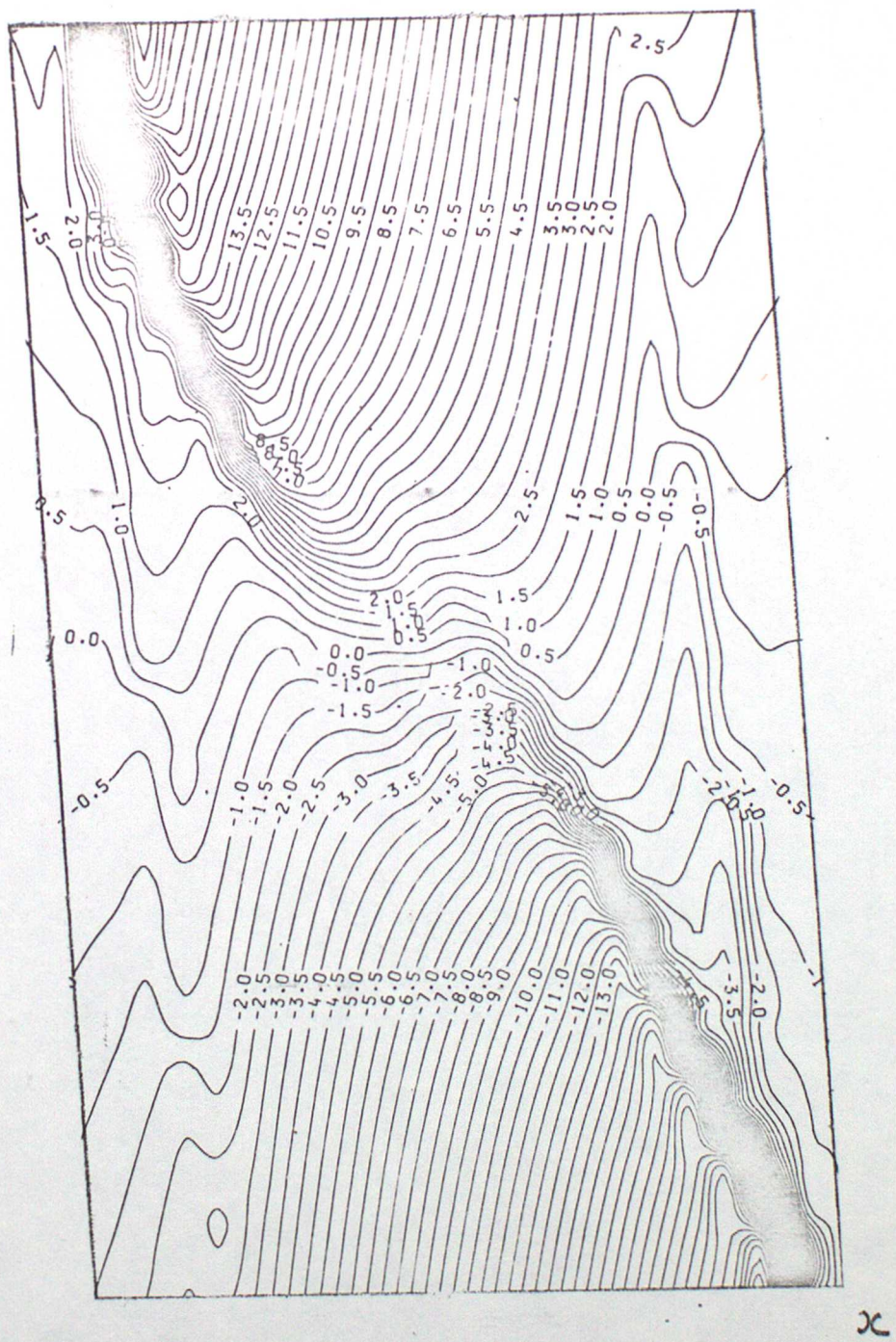

FIG. 2

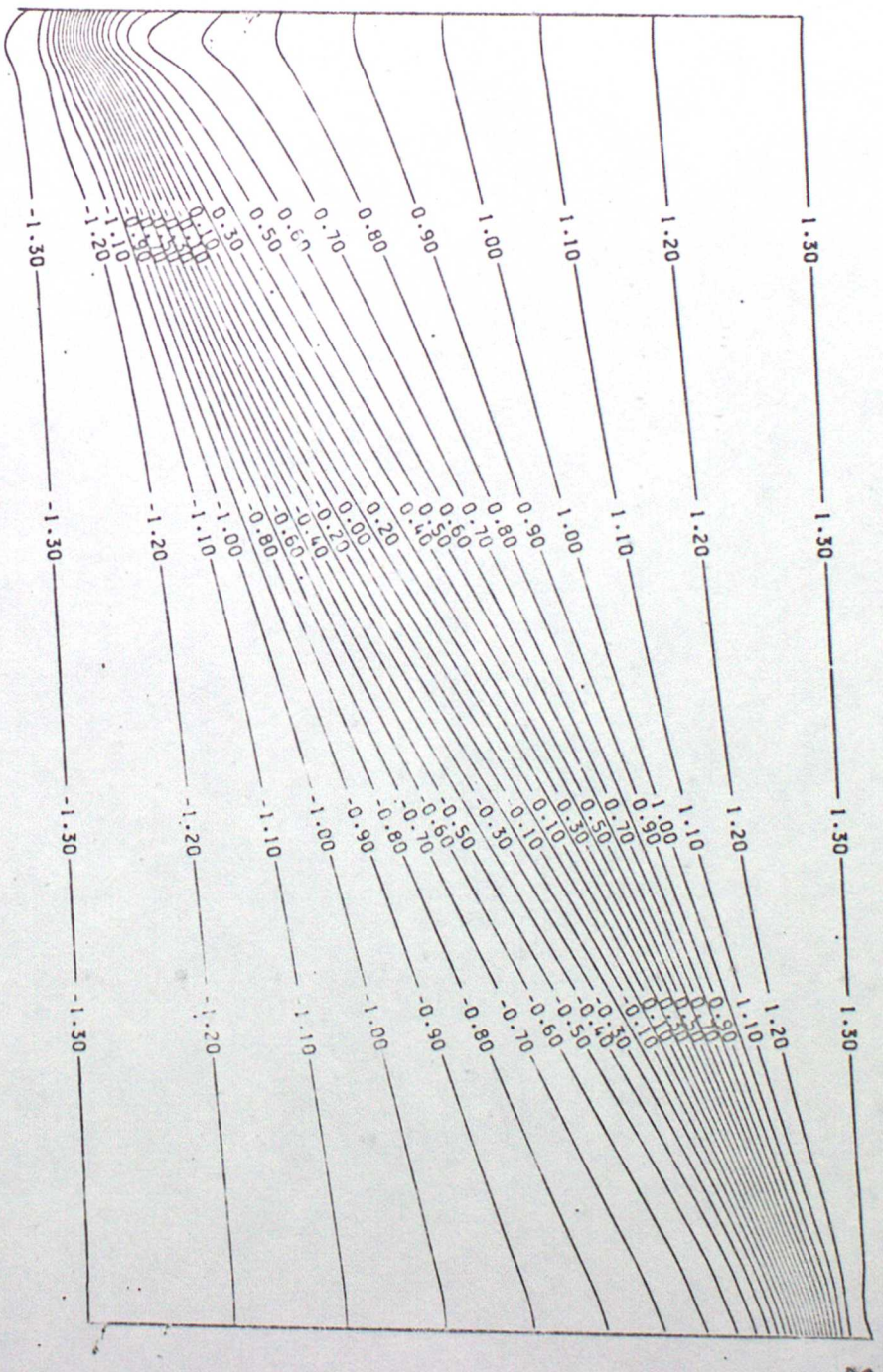
3
1.30
1.20
1.10
1.00
0.90
0.80
0.70
0.60
0.50
0.30
0.20
0.00
-0.20
-0.40
-0.60
-0.80
-1.00
-1.10
-1.20
-1.30
X

FIG. 3

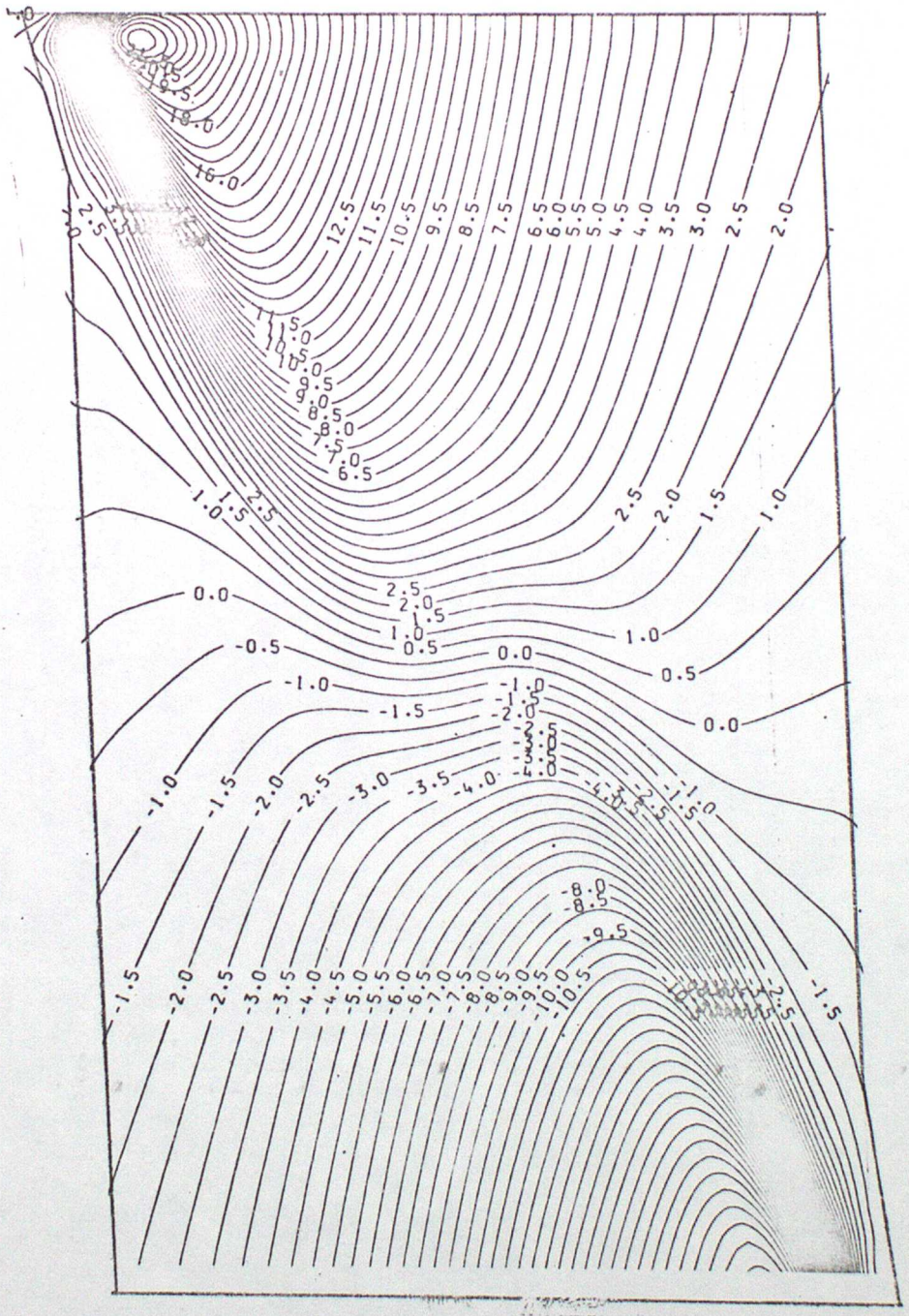

FIG. 4

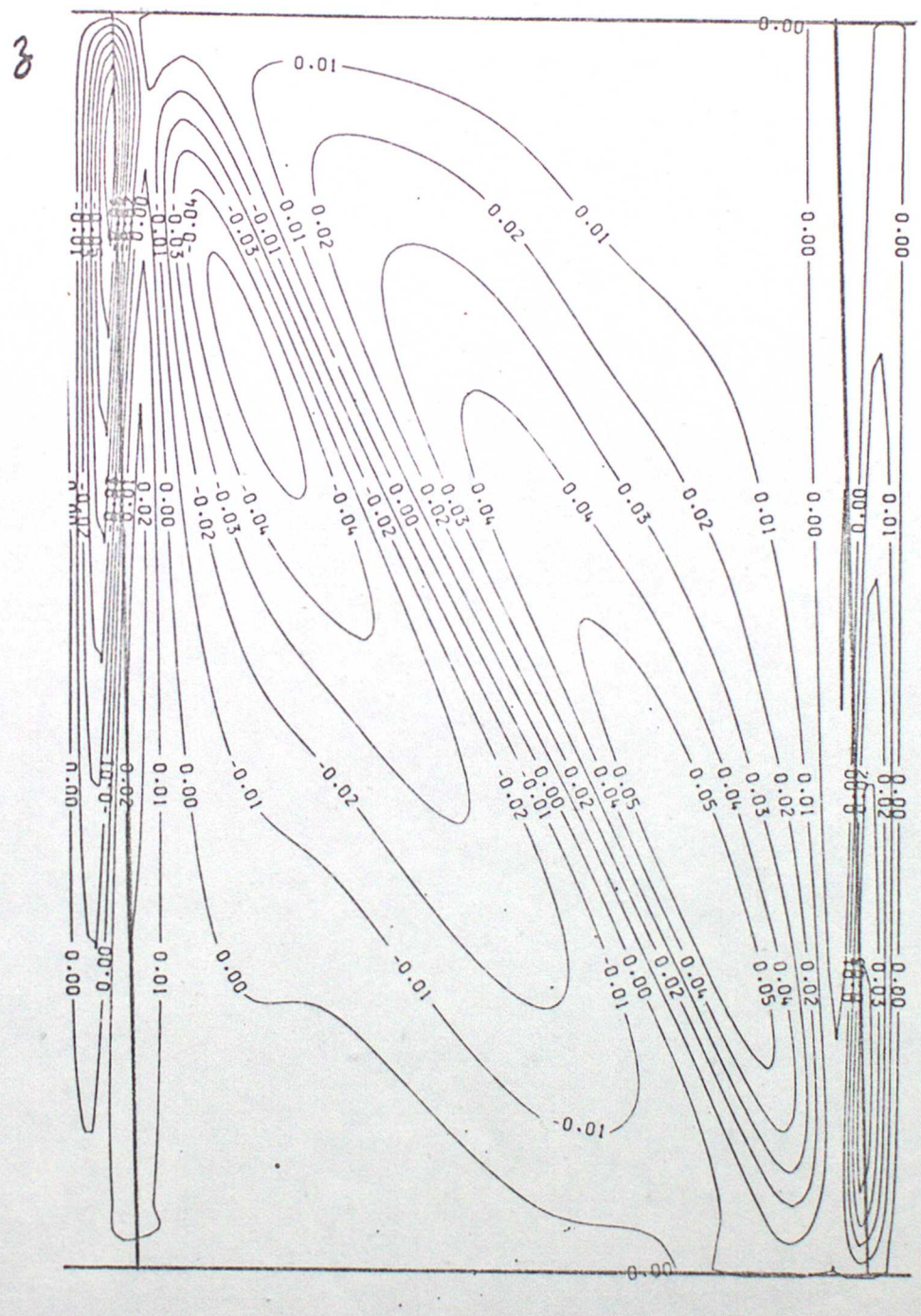

FIG. 5

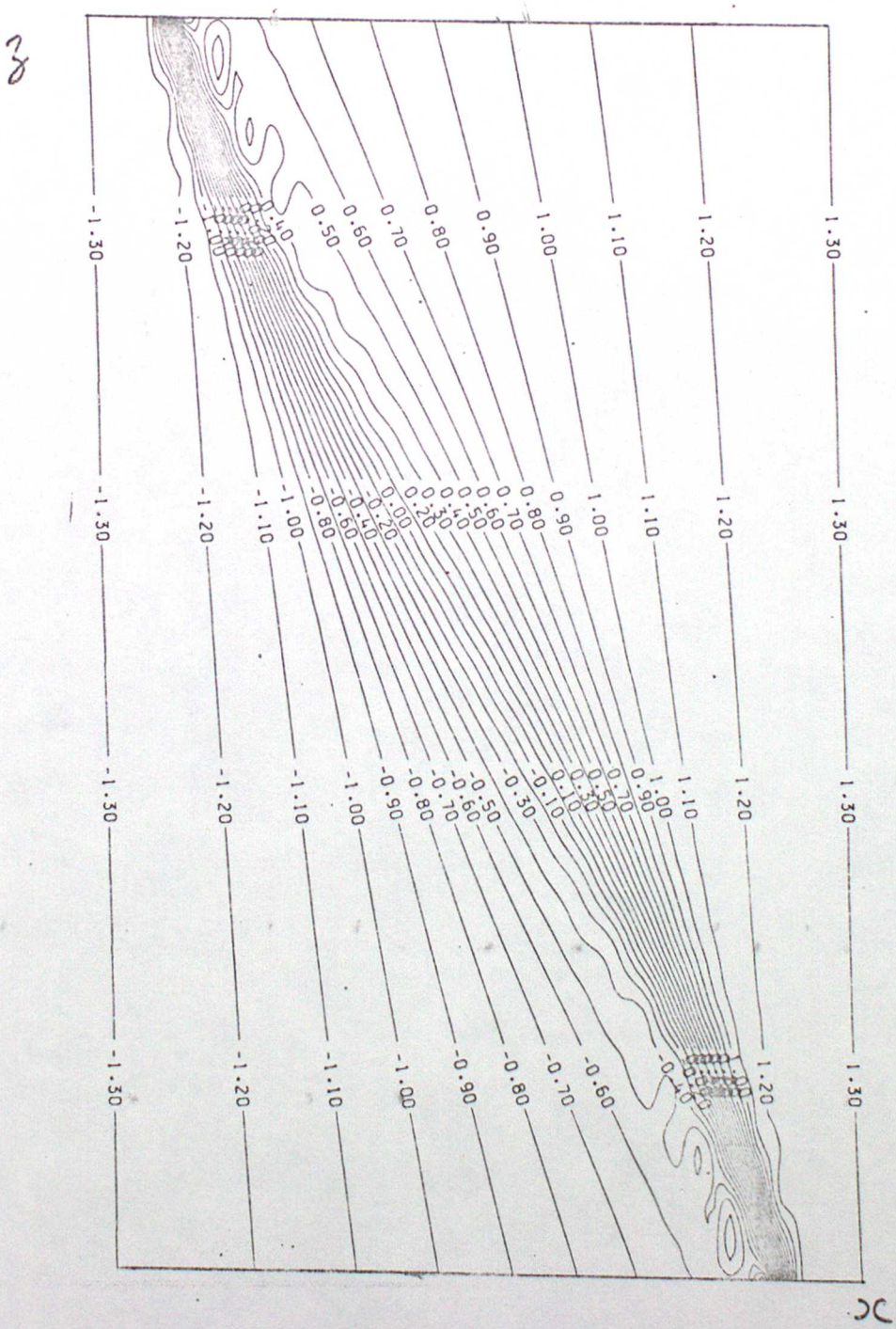
y
x
1.30
1.20
1.10
1.00
0.90
0.80
0.70
0.60
0.50
0.40
0.30
0.20
0.10
0.00
-0.10
-0.20
-0.30
-0.40
-0.50
-0.60
-0.70
-0.80
-0.90
-1.00
-1.10
-1.20
-1.30

FIG. 6

3

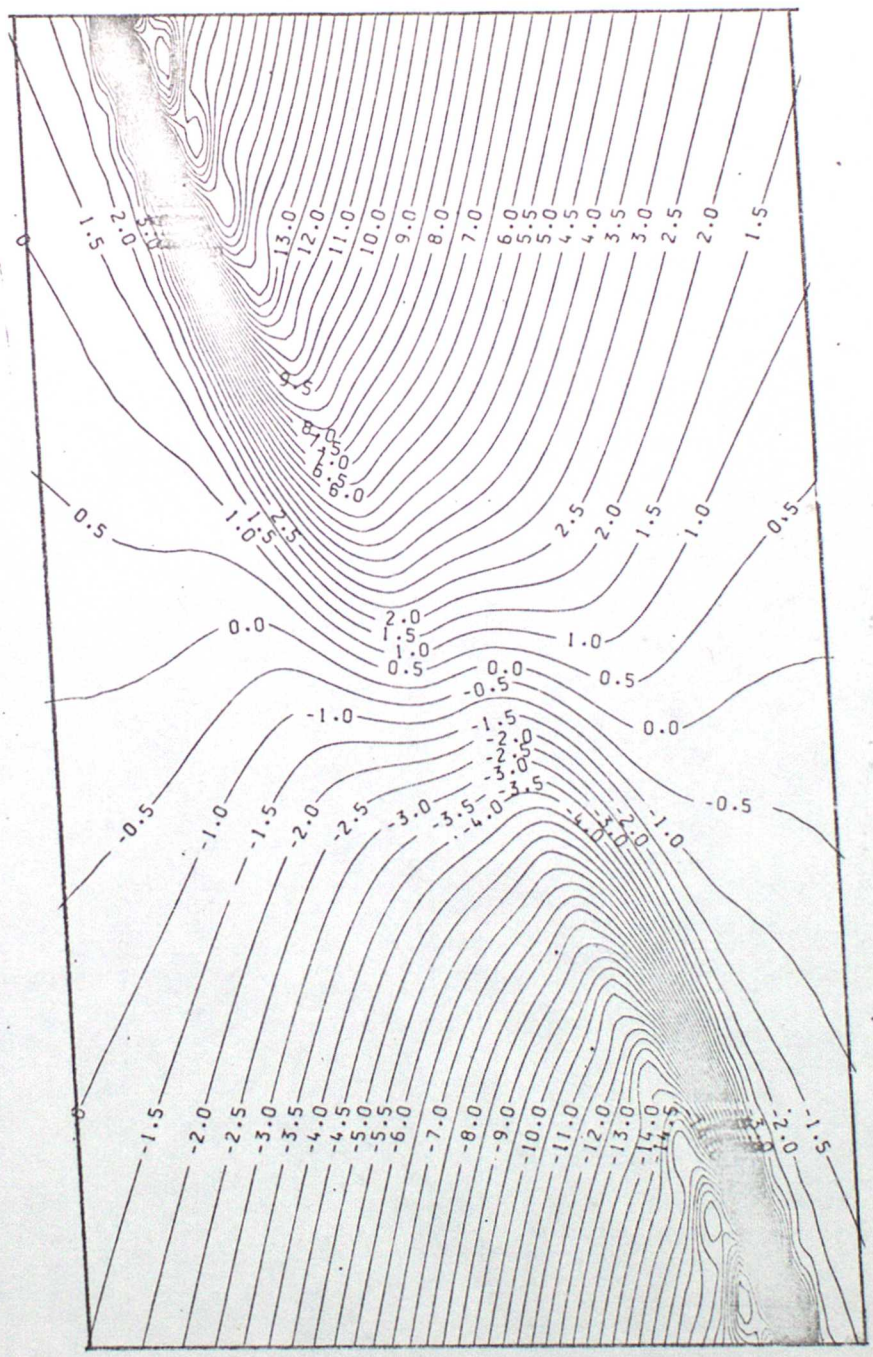
13.0
12.0
11.0
10.0
9.0
8.0
7.0
6.0
5.5
5.0
4.5
4.0
3.5
3.0
2.5
2.0
1.5
1.0
0.5
0.0
-0.5
-1.0
-1.5
-2.0
-2.5
-3.0
-3.5
-4.0
-4.5
-5.0
-5.5
-6.0
-7.0
-8.0
-9.0
-10.0
-11.0
-12.0
-13.0
-14.0
-14.5

x

FIG. 7

FIG. 8

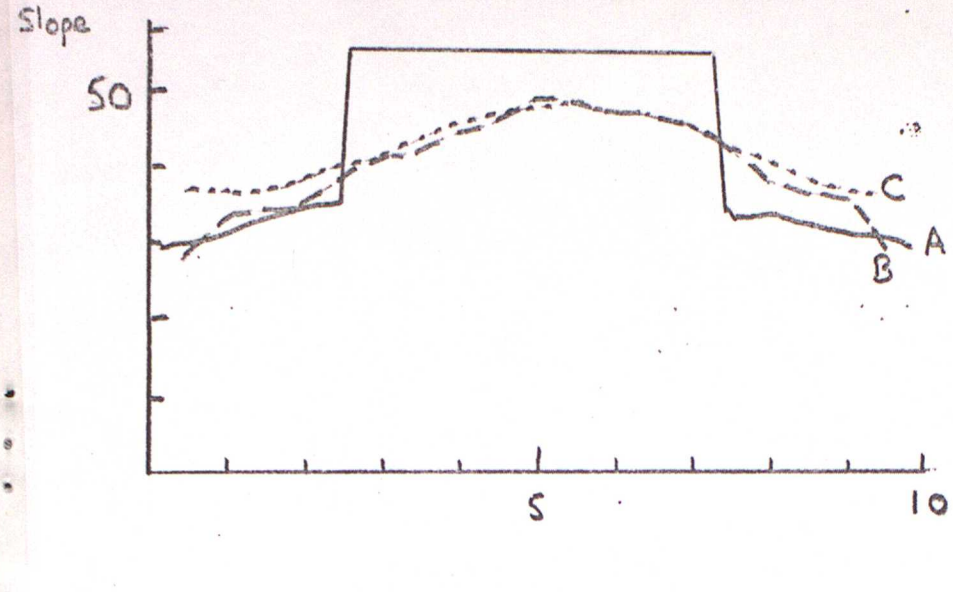
Slope
50
C
A
B
5
10
$z \times 10^{-3}$

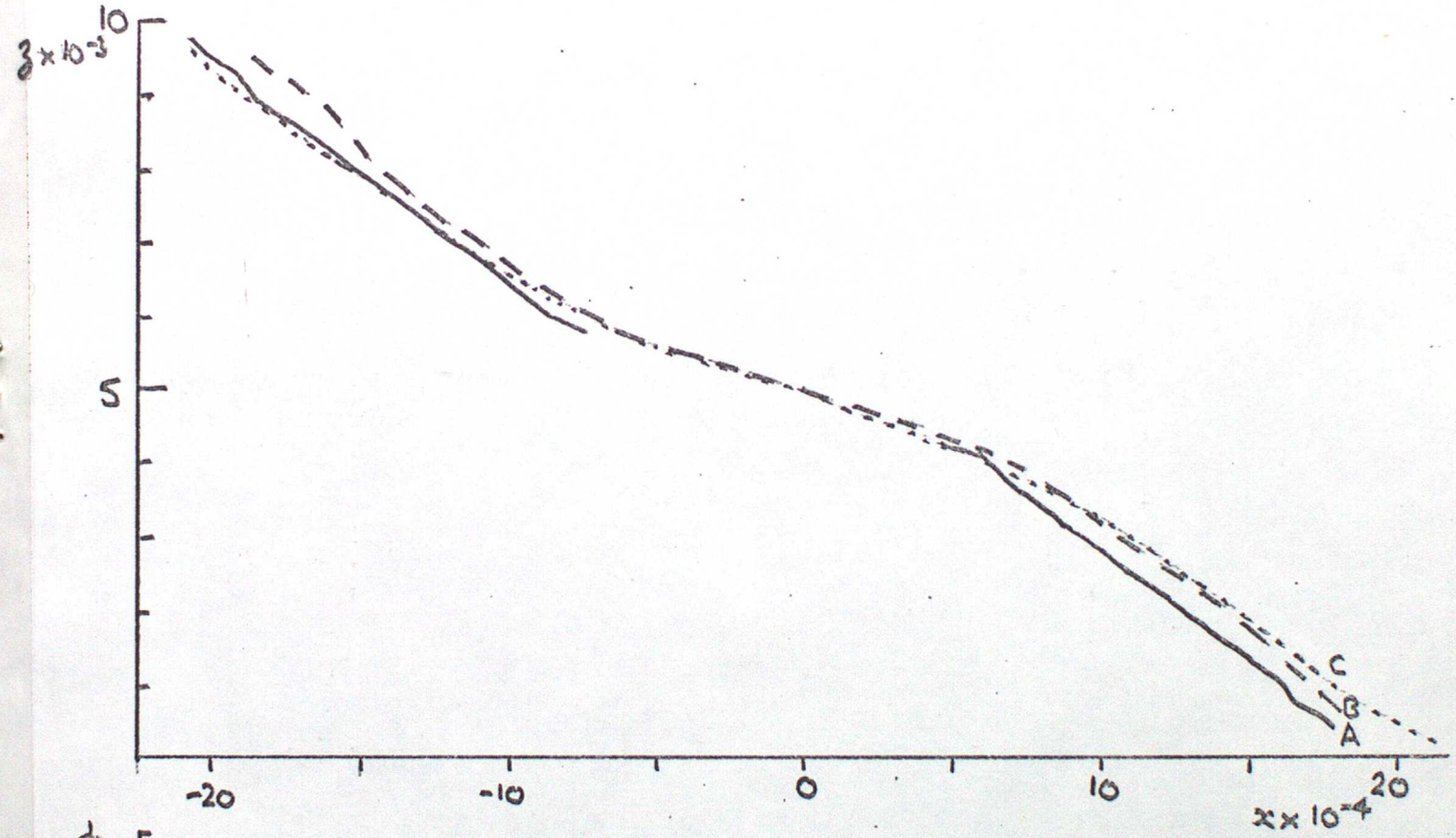
$z \times 10^{-3}$
10
5
C
B
A
-20
-10
0
10
20
$x \times 10^{-4}$

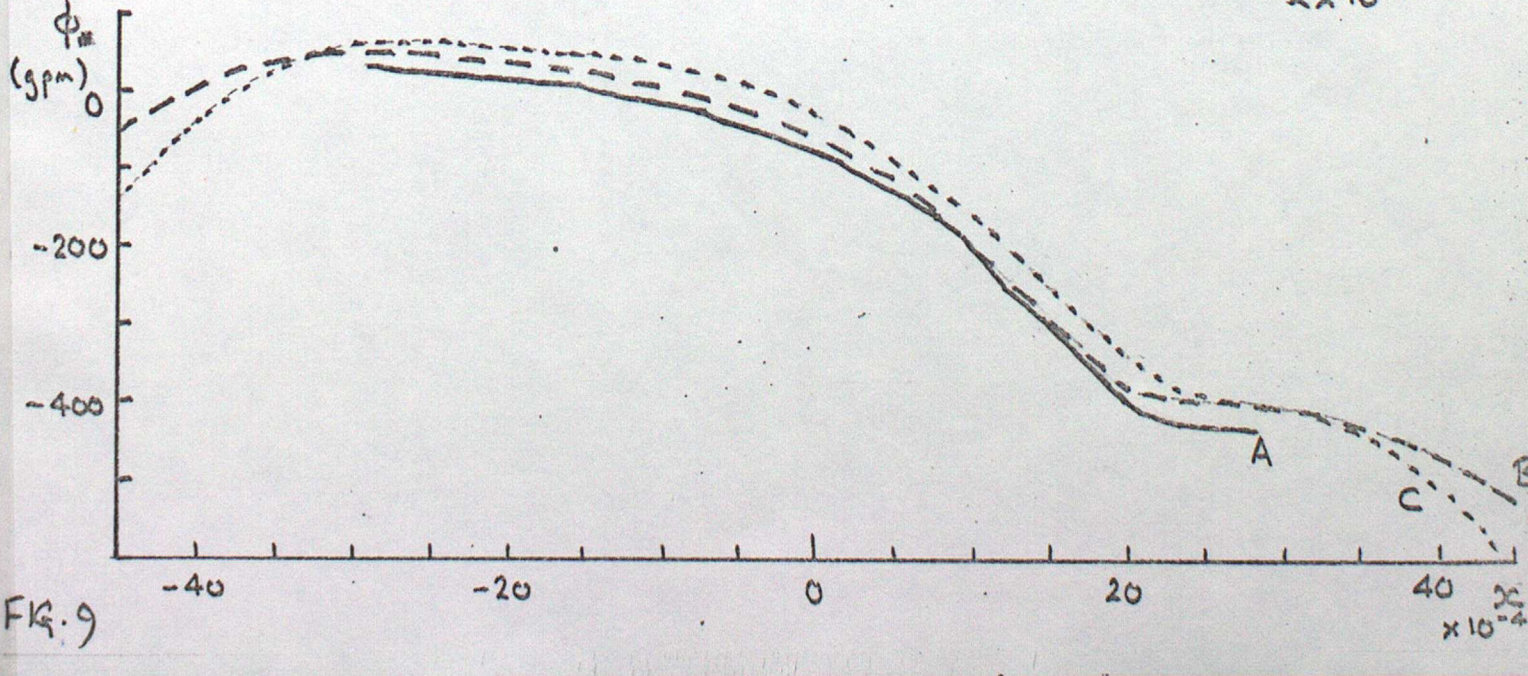
ϕ_m
(gpm)
0
-200
-400
A
B
C
-40
-20
0
20
40
$x \times 10^{-4}$

FIG. 9

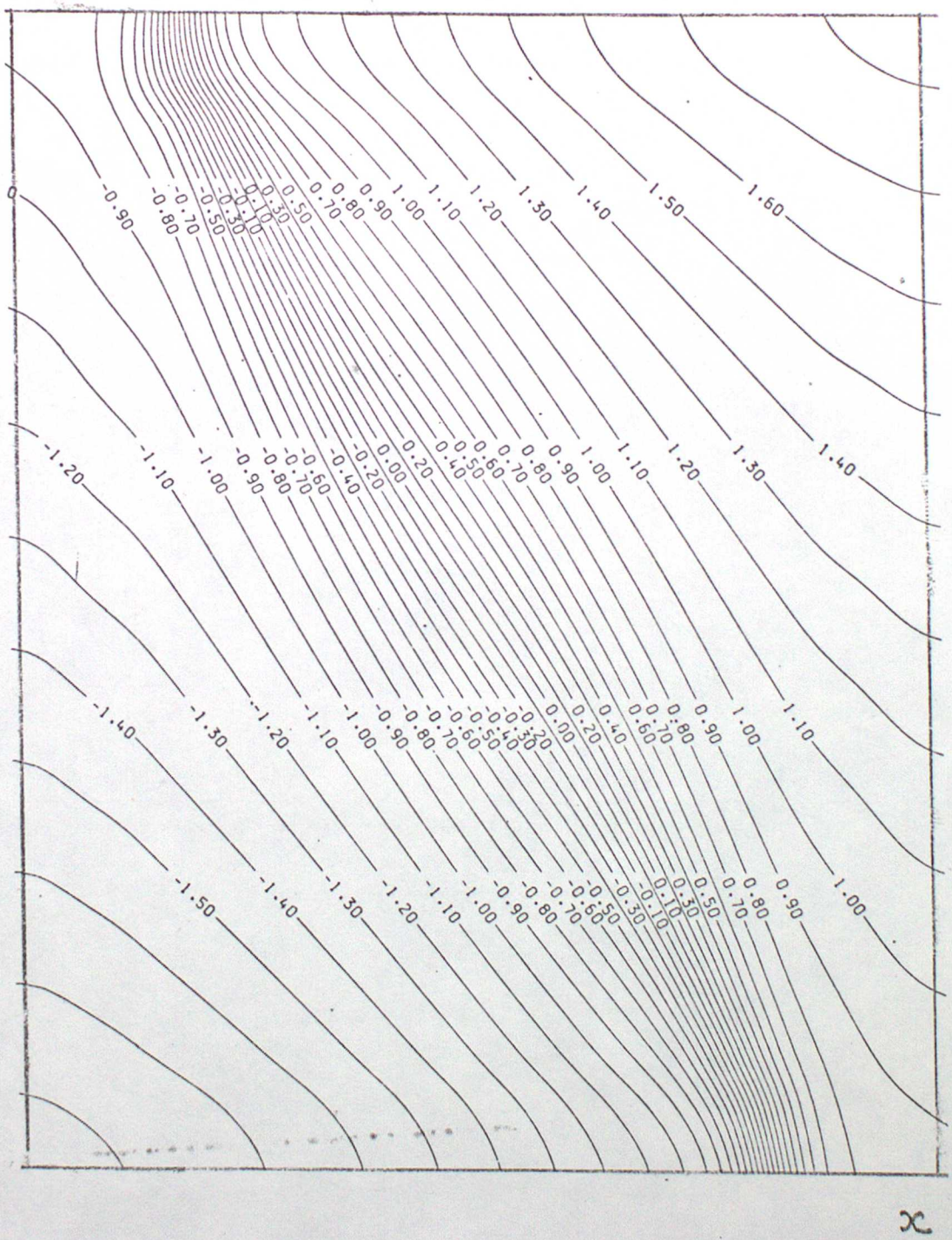
z
x
0
-0.90
-0.80
-0.70
-0.50
-0.30
-0.10
0.10
0.30
0.50
0.70
0.80
0.90
1.00
1.10
1.20
1.30
1.40
1.50
1.60
-1.20
-1.10
-1.00
-0.90
-0.80
-0.70
-0.60
-0.50
-0.40
-0.20
0.00
0.20
0.40
0.50
0.60
0.70
0.80
0.90
1.00
1.10
1.20
1.30
1.40
-1.40
-1.30
-1.20
-1.10
-1.00
-0.90
-0.80
-0.70
-0.60
-0.50
-0.40
-0.30
-0.20
0.00
0.20
0.40
0.60
0.70
0.80
0.90
1.00
1.10
-1.50
-1.40
-1.30
-1.20
-1.10
-1.00
-0.90
-0.80
-0.70
-0.60
-0.50
-0.30
-0.10
0.10
0.30
0.50
0.70
0.80
0.90
1.00

FIG. 10

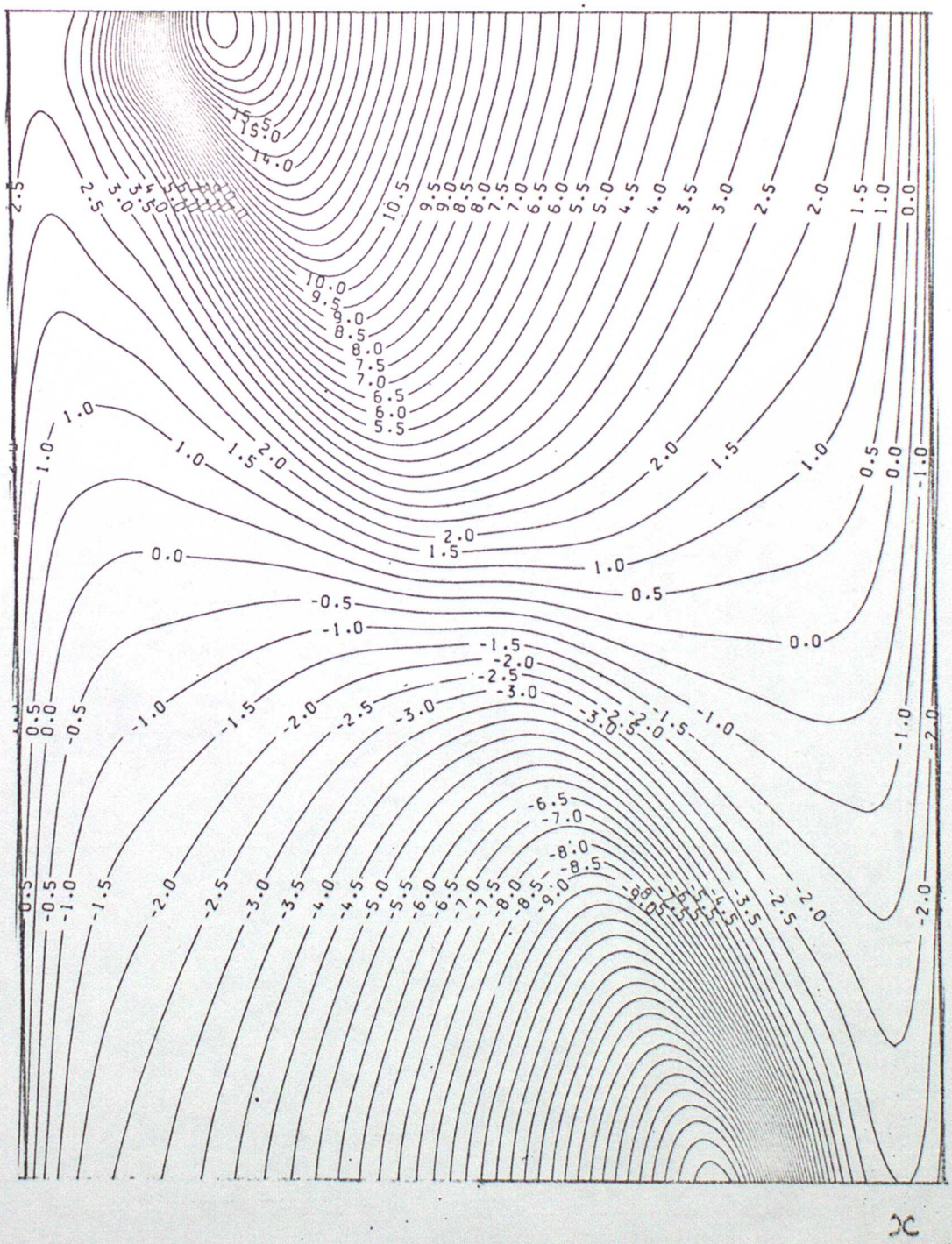

FIG. 11

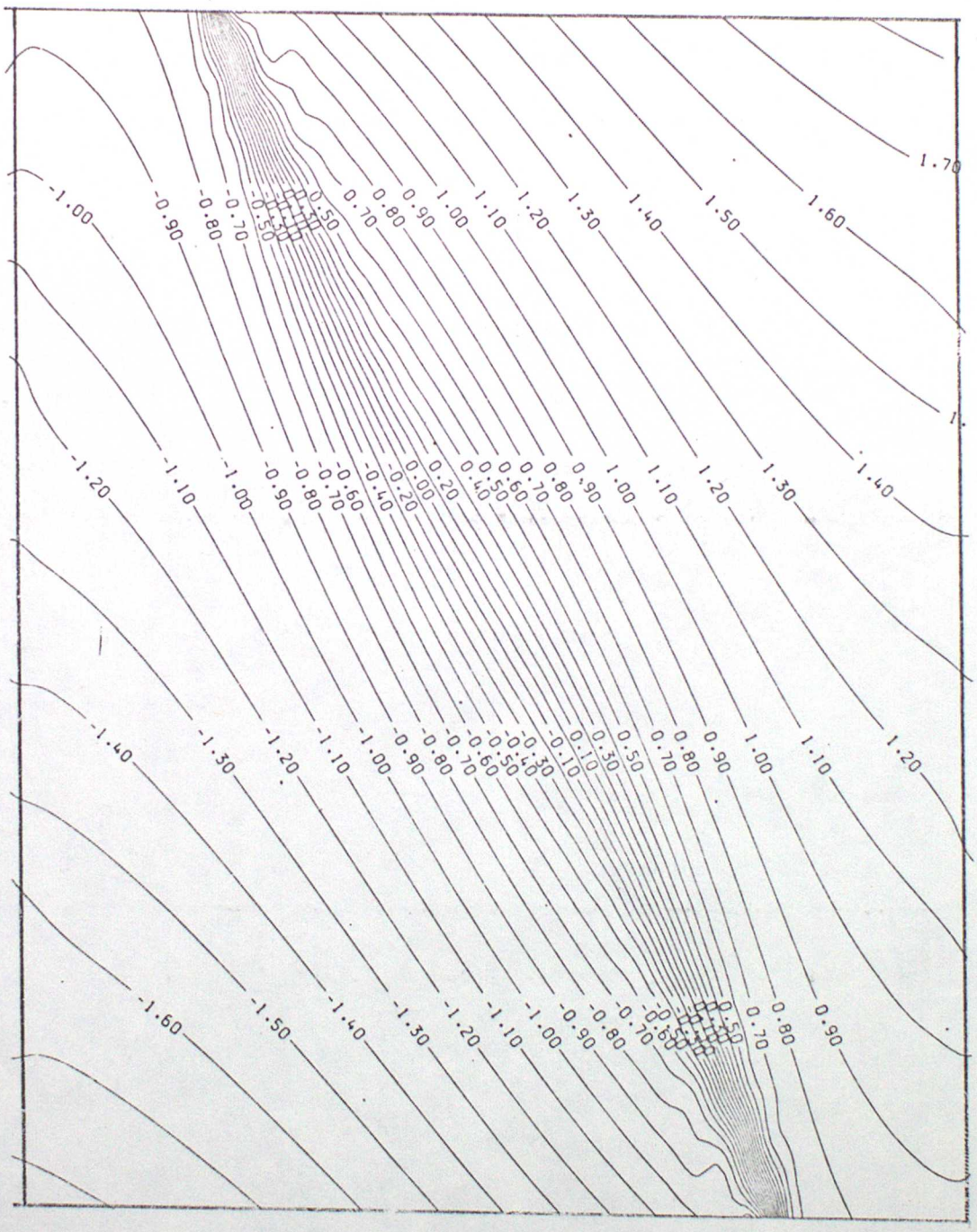
z
x
1.70
1.60
1.50
1.40
1.30
1.20
1.10
1.00
0.90
0.80
0.70
0.60
0.50
0.40
0.30
0.20
0.10
0.00
-0.10
-0.20
-0.30
-0.40
-0.50
-0.60
-0.70
-0.80
-0.90
-1.00
-1.10
-1.20
-1.30
-1.40
-1.50
-1.60

FIG. 12

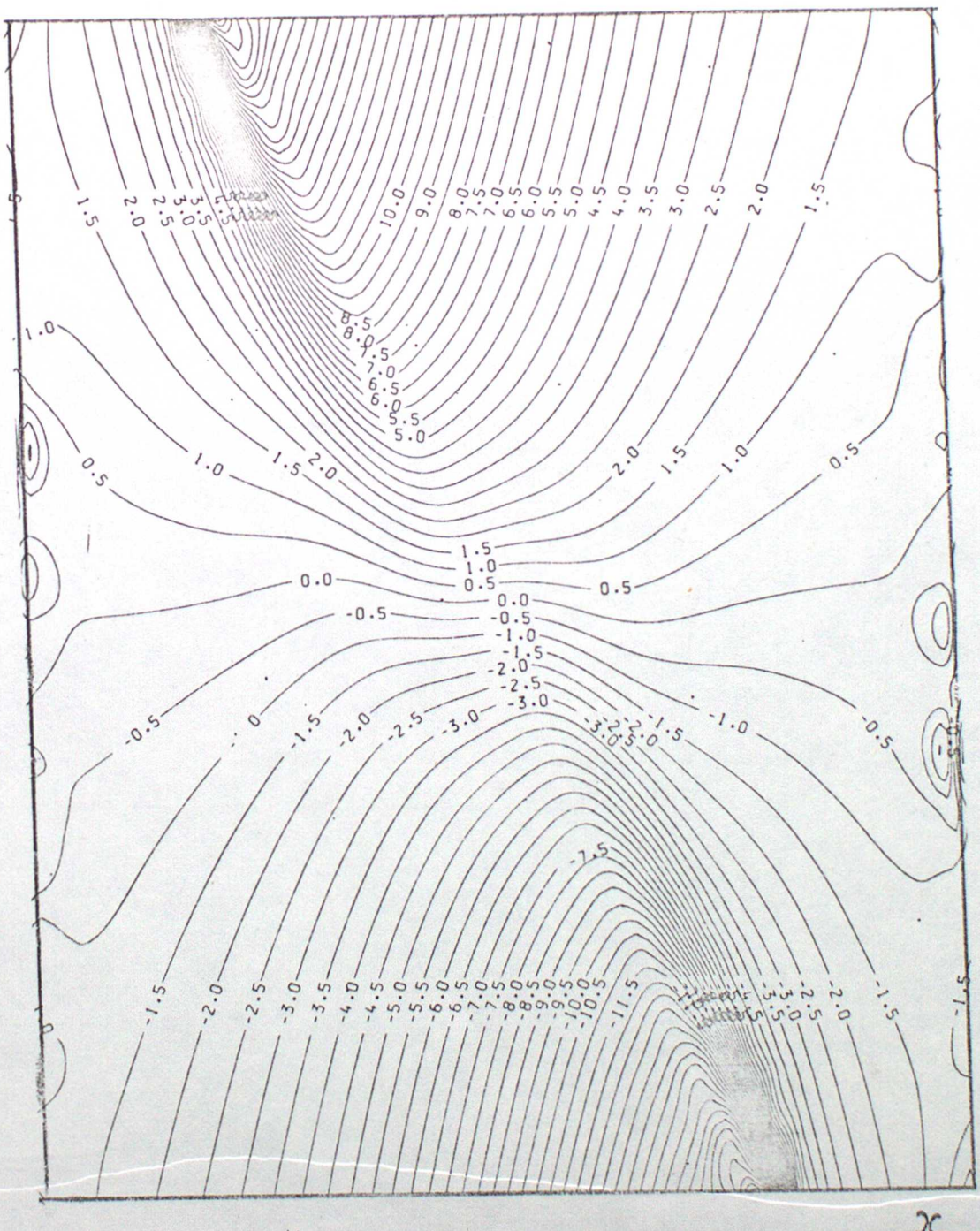

FIG. 13

3

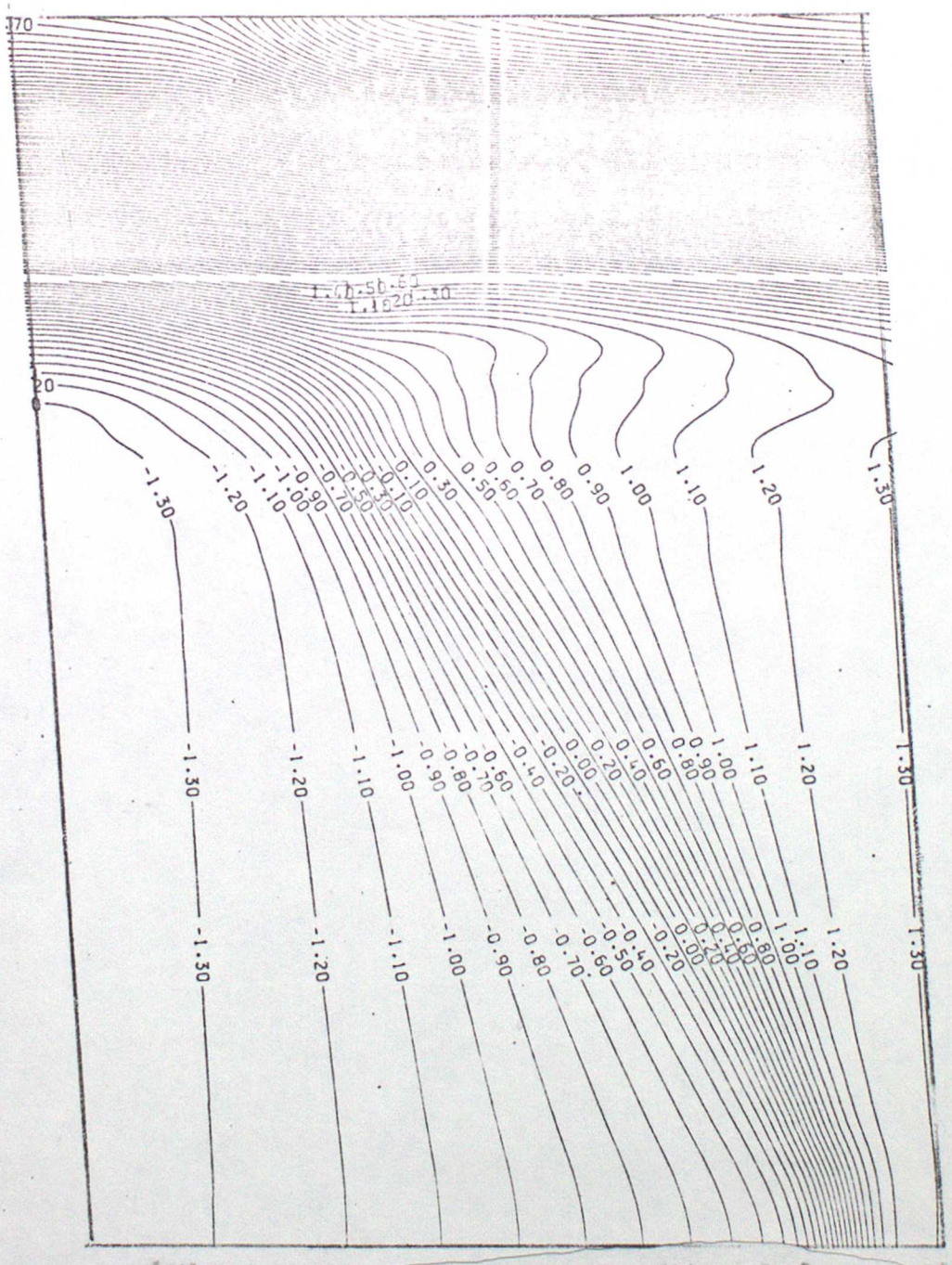
1.70
1.60
1.50
1.40
1.30
1.20
1.10
1.00
0.90
0.80
0.70
0.60
0.50
0.40
0.30
0.20
0.10
0.00
-0.10
-0.20
-0.30
-0.40
-0.50
-0.60
-0.70
-0.80
-0.90
-1.00
-1.10
-1.20
-1.30
x

FIG. 14

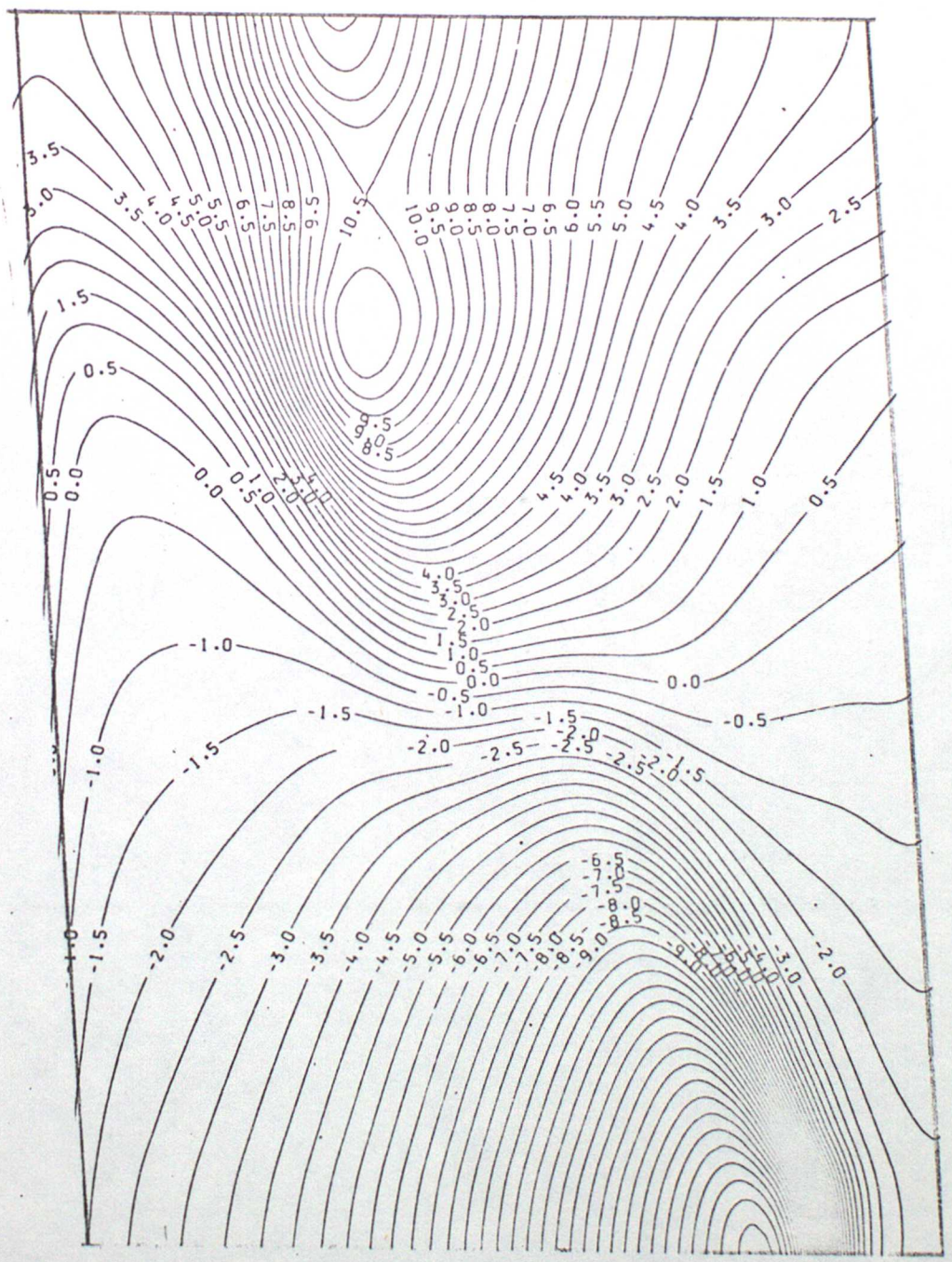

FIG. 15

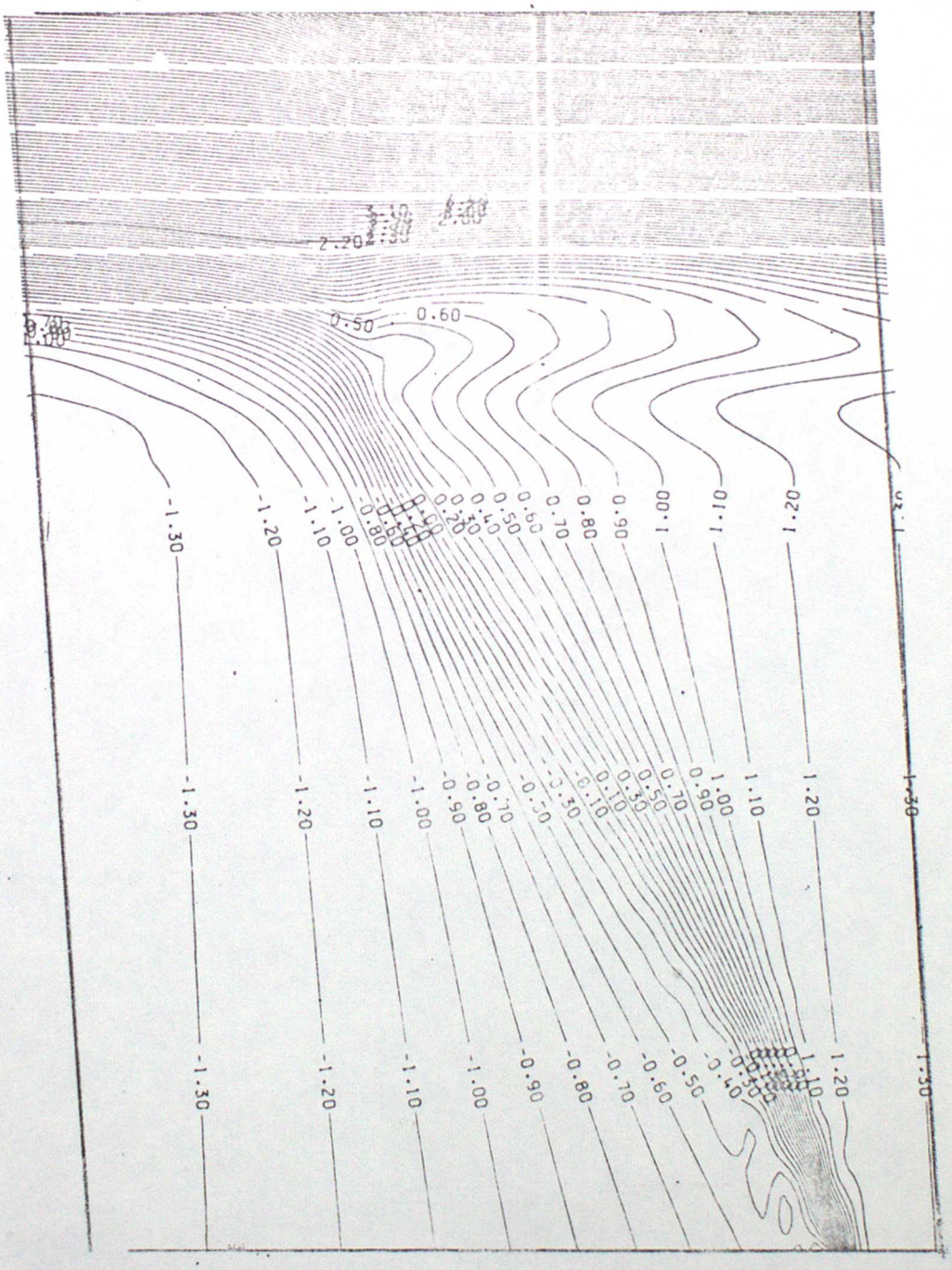
3
2.20
0.50
0.60
0.80
0.90
1.00
1.10
1.20
1.30
-1.30
-1.20
-1.10
-1.00
-0.90
-0.80
-0.70
-0.60
-0.50
-0.40
-0.30
-0.20
-0.10
0.10
0.30
0.40
0.50
0.60
0.70
x

FIG. 16

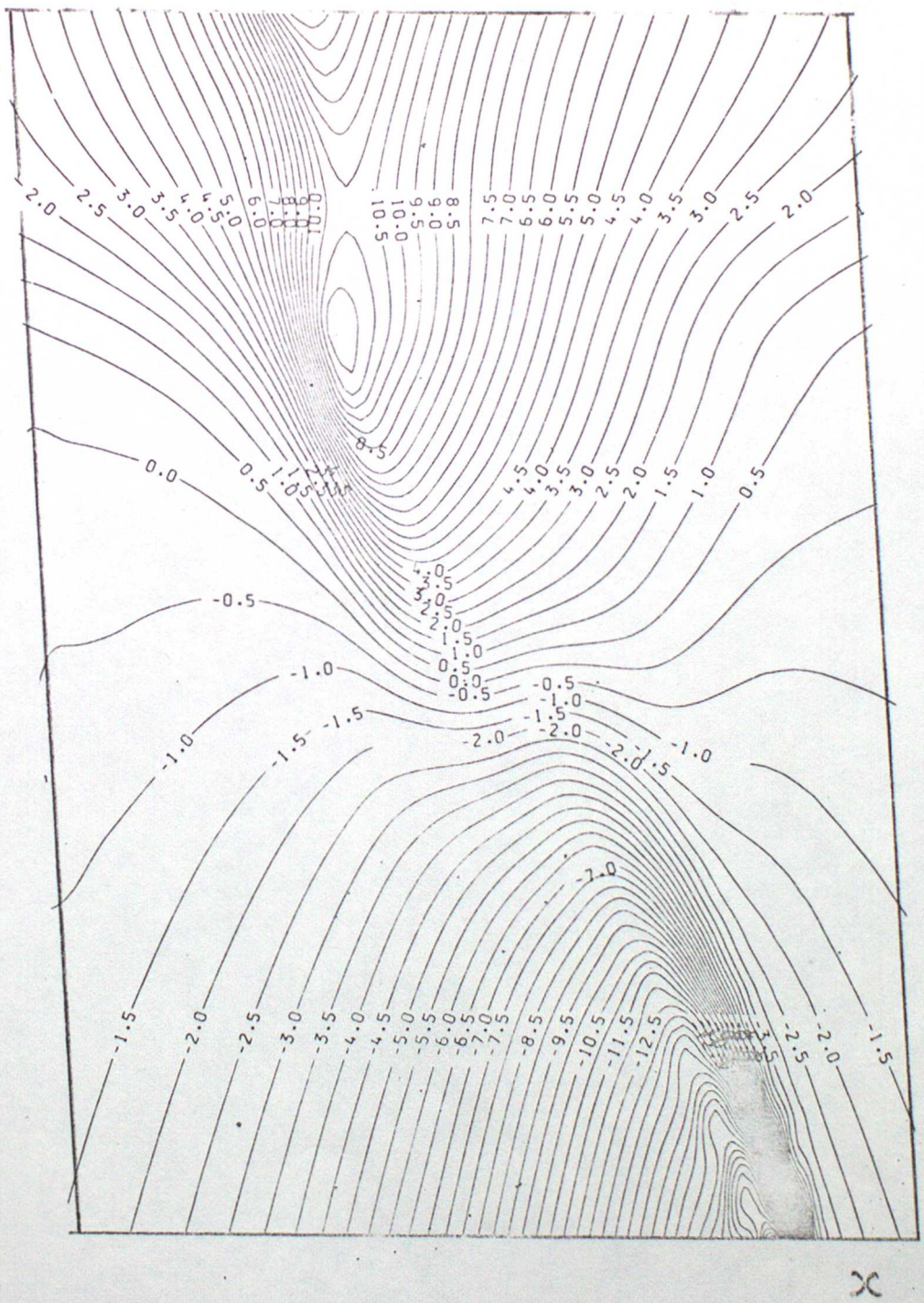

FIG. 17